J|A|C|S COMMUNICATIONS

Published on Web 01/29/2009

Reversible Switching of Magnetism in Thiolate-Protected Au_{25} Superatoms

Manzhou Zhu,[†] Christine M. Aikens,[‡] Michael P. Hendrich,[†] Rupal Gupta,[†] Huifeng Qian,[†] George C. Schatz,[§] and Rongchao Jin*,[†]

Department of Chemistry, Carnegie Mellon University, 4400 Fifth Avenue, Pittsburgh, Pennsylvania 15213, Department of Chemistry, Kansas State University, Manhattan, Kansas 66506, and Department of Chemistry, Northwestern University, Evanston, Illinois 60208

Received November 23, 2008; E-mail: rongchao@andrew.cmu.edu

Single gold atoms (e.g., in gas beams or adsorbed on a support) are paramagnetic because of the unpaired 6s electron, while bulk gold is diamagnetic because the paramagnetism of the conduction electrons is counteracted by the orbital and ionic core diamagnetism.[1] The evolution of magnetism in going from gold atoms to nanoparticles to the bulk is of fundamental interest and importance. Previous work has observed magnetism in small Au nanoparticles,[2−8] and a size-dependent magnetization was found for ∼1−5 nm Au nanoparticles.[4] However, contradictory results exist in the literature, as the nanoparticle size distribution and ill-defined surface properties complicate the interpretation. Therefore, it is of critical importance to create a well-defined nanoparticle system and to achieve crystal-structure−property correlations in order to study the fundamentals of magnetism in gold nanoparticles.

We report reversible switching of paramagnetism in this first study of a well-defined gold nanoparticle system consisting of truly monodisperse nanoparticles containing 25 gold atoms stabilized by 18 thiolate ligands [abbreviated as $Au_{25}(SR)_{18}$, where R = phenylethyl]. Density functional theory (DFT) calculations successfully explain the origin of the magnetism, and it is found that the unpaired spin in the $Au_{25}(SR)_{18}$ nanoparticle resides in the Kohn−Sham highest occupied molecular orbital (HOMO). Interestingly, the HOMO orbital exhibits distinct P-like character, reminiscent of the superatom model for bare metal clusters.[9−12] The results of this work demonstrate that the $Au_{25}(SR)_{18}$ nanoparticle is best considered as a ligand-protected superatom.

The $Au_{25}(SR)_{18}$ nanoparticles were synthesized via a kinetically controlled synthetic approach.[13] The as-prepared gold nanoparticles were precipitated with ethanol and recrystallized in a mixed toluene/ethanol solvent. In this work, the collected Au_{25} nanoparticles were further reacted with H_2O_2 (33%, aqueous). X-ray crystallographic analysis showed that the oxidized product consists of charge-neutral $[Au_{25}(SR)_{18}]^0$ nanoparticles.[14] The $[Au_{25}(SR)_{18}]^0$ structure is based on an icosahedral Au_{13} core, which is capped by a second gold shell comprising the remaining 12 Au atoms. In another view, the particle can be regarded as an Au_{13} core capped by six "staple" motifs (−S−Au−S−Au−S−).

The magnetic properties of these well-defined, atomically monodisperse Au_{25} nanoparticles were evaluated with electron paramagnetic resonance (EPR) spectroscopy using microcrystal powders of the nanoparticles (see the Supporting Information for experimental details). Low-temperature EPR spectra of the as-prepared $[Au_{25}(SR)_{18}]^0$ particles are shown in Figure 1. Microcrystalline and frozen-solution samples show an $S = {}^1/_2$ signal with $\mathbf{g}$ = (2.56, 2.36, 1.82). EPR quantification of both samples indicates that $[Au_{25}(SR)_{18}]^0$ has one unpaired spin per particle. Solution samples

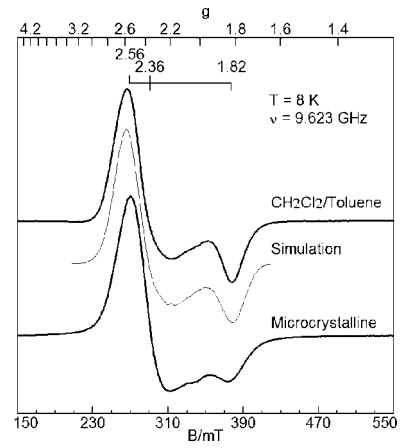

Figure 1. EPR spectra of $[Au_{25}(SR)_{18}]^0$ for the conditions listed. Simulation parameters: $\mathbf{g}$ = (2.556, 2.364, 1.821), g strain (σ_g) = 0.03, 13 equivalent $I = {}^3/_2$ nuclei with $\mathbf{A}$ = (71, 142, 50) MHz.

prepared in toluene, chloroform, or 1:1 CH_2Cl_2/toluene over the concentration range of 1−0.01 mM $[Au_{25}(SR)_{18}]^0$ all show the same signal with no discernible change in line width. Surprisingly, there is no evidence of hyperfine splitting from the ^{197}Au nuclei ($I = {}^3/_2$, natural abundance 100%) in any of these samples. Decreasing the amplitude of the magnetic field modulation has no effect on the line shape. The signal is not easily saturated: at 8 K with 200 mW of microwave power, the signal amplitude is reduced by at most 15% from the nonsaturation regime, for which amplitude ∼ (power)$^{1/2}$. At higher temperatures (>100 K), the EPR signal begins to broaden, and at room temperature, no signal is detectable. This is due to lifetime broadening of the signal, since the amount of material (∼5 mg of microcrystal powder) was sufficient to detect a signal at room temperature in the absence of line broadening. Magnetization measurements using a superconducting quantum interference device (SQUID) magnetometer also reveal that these nanoparticles are paramagnetic between 5 and 300 K, and no hysteresis was observed at 5 K.

It is interesting to note that the EPR signal disappeared after the $[Au_{25}(SR)_{18}]^0$ nanoparticles were treated with a reducing agent (aqueous $NaBH_4$). The reduced nanoparticles were determined to be an anionic form of the Au_{25} nanoparticle, $[Au_{25}(SR)_{18}]^-$, which has a structure similar to that of the $[Au_{25}(SR)_{18}]^0$ particle except for the charge state.[13,14] When the $[Au_{25}(SR)_{18}]^-$ nanoparticles were treated again with H_2O_2, the EPR signal was recovered. Therefore, the paramagnetism in the Au_{25} nanoparticles can be switched on or off simply by controlling the charge state of the nanoparticle (Figure 2A). This reversible switching behavior is indeed quite intriguing, and it is of particular importance to find out the origin of the magnetism in these gold nanoparticles. The possibility that

[†] Carnegie Mellon University.
[‡] Kansas State University.
[§] Northwestern University.

10.1021/ja809157f CCC: $40.75

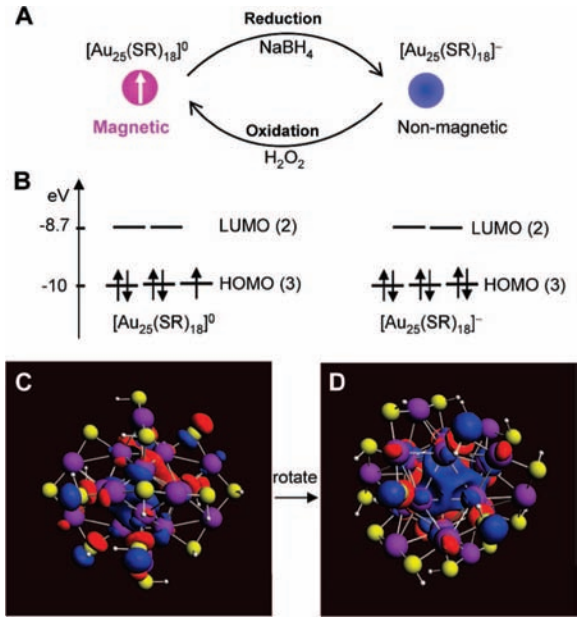

Figure 2. (A) Reversible conversion between the neutral and anionic $Au_{25}(SR)_{18}$ nanoparticles. (B) DFT-calculated Kohn−Sham orbital energy-level diagrams for the neutral and anionic nanoparticles, respectively. (C−D) Views of the Kohn−Sham HOMO for $[Au_{25}(SH)_{18}]^0$ at the LB94//Xα/TZP level of theory. The HOMO possesses two lobes and exhibits distinct P-like character. (D) is rotated relative to (C) to show one of the lobes (contributed by three Au atoms in the icosahedral shell). Color code: purple, Au; yellow, S; white, H.

the paramagnetism originates from magnetic impurities, such as Fe, Co, or Ni species or organic radicals, is ruled out because the EPR signal intensity is quantitatively correct for one spin per particle. Pauli paramagnetism is also ruled out because this bulk metal effect would give only a very weak paramagnetism in gold.

To account for the intrinsic magnetism of the $Au_{25}(SR)_{18}$ nanoparticles, we performed DFT calculations for a model $Au_{25}(SH)_{18}$ nanoparticle. These DFT calculations reveal that for both the neutral and anionic particles, the HOMO level is approximately triply degenerate while the LUMO is doubly degenerate (Figure 2B). The electronic configuration for the neutral particle's HOMO orbitals is $(a_u)^2(a_u)^2(a_u)^1$. The orbital energies of these three orbitals are predicted to be −9.65, −9.54, and −9.33 eV, respectively, for $Au_{25}(SH)_{18}{}^0$ at the spin−orbit-coupled LB94/TZP level of theory; thus, the energies are very slightly split, and the highest-energy orbital in the HOMO set is singly occupied. The presence of one unpaired electron in the HOMO of the neutral state explicitly explains the paramagnetism observed in both the EPR and SQUID measurements and also agrees with the quantitative result, i.e., one spin per particle. In contrast, for the $[Au_{25}(SR)_{18}]^-$ nanoparticle, the three quasidegenerate Kohn−Sham orbitals are completely filled, giving the $(a_u)^2(a_u)^2(a_u)^2$ configuration (Figure 2B). The absence of unpaired electrons in the HOMO level explains why the EPR signal disappears for $[Au_{25}(SR)_{18}]^-$.

The observed $[Au_{25}(SR)_{18}]^0$ resonances, $\mathbf{g} = (2.56, 2.36, 1.82)$, with the significant shift from $g = 2$, are unprecedented for Au complexes. Large shifts have previously been observed for ethylene−Au complexes and attributed to the presence of low-lying orbitals and the large spin−orbit coupling constant for Au (2544 cm^{-1}).[15] The DFT-calculated **g** tensor for $[Au_{25}(SH)_{18}]^0$, $\mathbf{g} = (2.511, 2.386, 1.826)$, is indeed in excellent agreement with the experimental results. The quasidegenerate configuration of the HOMO orbital of $[Au_{25}(SR)_{18}]^0$ produces a large orbital contribution to the **g** tensor through enhanced spin−orbit coupling. The mean value of the orbital angular momentum would vanish if the particle did not have orbitally degenerate ground states.

The approximate axial symmetry observed in the EPR experiment can be explained by considering a superatom model of the nanoparticle. The $[Au_{25}(SR)_{18}]^-$ anion may be viewed as containing eight delocalized electrons in an icosahedral core, which is a common magic number for superatom clusters.[16] (It should be noted that the 18 thiolate ligands formally consume 18 of the 25 gold 6s valence electrons.) Projection of the triply degenerate HOMO electronic states onto spherical harmonics shows that the HOMO level has P character;[16] hence, an electronic shell structure of $1S^21P^6$ is predicted for the anionic nanoparticle. The corresponding neutral particle, $[Au_{25}(SH)_{18}]^0$, is expected to have an electronic shell structure of $1S^21P^5$, which exhibits the axial symmetry of the unfilled P shell (Figure 2C,D). The singly occupied P orbital possesses two lobes and a node at the center of the icosahedral core, and each lobe involves three gold atoms in the icosahedral shell (Figure 2D). The electron density falls primarily in the Au_{13} core and is mainly contributed by the Au 6s atomic orbitals in the Au_{13} core (with some contribution from 3p electrons on the sulfur atoms).

The absence of hyperfine splitting in the EPR spectra of $[Au_{25}(SR)_{18}]^0$ is remarkable given the large number of Au atoms in the particle. Free atomic Au^0 with a valence $6s^1$ configuration has a large hyperfine coupling constant from the ^{197}Au nucleus ($I = {}^3/_2$) of $A_{iso} = 3138$ MHz.[17] Isolated Au^0 adsorbed onto MgO films displays an $S = {}^1/_2$ signal with $\mathbf{g} = (2.07, 2.07, 1.99)$ and a large isotropic hyperfine constant of $A_{iso} = 1405$ MHz.[18] Small organic complexes (e.g., with ethylene) of trapped Au^0 in an argon matrix show either a large hyperfine constant [e.g., $A_{iso} = 1725$ MHz with a **g** tensor of (1.98, 1.95, 1.78) for monoethylene] or a much smaller value [e.g., $A_{iso} = 89$ MHz with a **g** tensor of (2.18, 1.98, 1.84) for bisethylene].[19] The reduction in the hyperfine interaction in going from monoethylene to bisethylene is due a switch in the orbital containing the unpaired electron (from Au sp_y in the case of monoethylene to Au p_x in the case of bisethylene).[19] The hyperfine splittings in the EPR spectra of solids can vanish as a result of exchange narrowing, but the absence of hyperfine features in the solution samples of $[Au_{25}(SR)_{18}]^0$ suggests this is not the cause. On the other hand, the hyperfine constant can be reduced significantly, as demonstrated by the mono- and bisethylene Au^0 complexes, when the unpaired electron occupies an orbital lacking significant s character[19] (i.e., the unpaired spin has a negligible spin density at the nucleus, so the Fermi contact contribution to A_{iso} disappears[1]).

To extract more information from the EPR results, we performed a simulation of the EPR spectrum for $[Au_{25}(SR)_{18}]^0$ in CH_2Cl_2/toluene (Figure 1, middle profile). This simulation employed an $S = {}^1/_2$ center with $\mathbf{g} = (2.56, 2.36, 1.82)$ and 13 equivalent Au nuclei from the inner core of the particle. For $A_{iso} \leq 100$ MHz, the simulation matches the experimental spectrum. This value is an upper limit; the inclusion of greater g strain (σ_g) combined with smaller values of the hyperfine constant does produce the same simulation. For $A_{iso} > 100$ MHz, either the line width is too broad or the simulation shows resolved hyperfine splitting from the 40 lines. The result is similar with inclusion of more Au nuclei. The DFT-calculated isotropic hyperfine coupling constant A_{iso} for $Au_{25}(SH)_{18}{}^0$ shows that the Au_{12} shell of the icosahedral core possesses the largest values, which range from 36.0 to 56.4 MHz (Table 1). In contrast, the gold atoms in the −S−Au−S−Au−S− staples and the central Au atom in the core have small hyperfine constants (<12.5 MHz; Table 1). Interestingly, the largest A_{iso} values in the 12-atom icosahedral shell of the Au_{13} core correspond to

Table 1. Isotropic Hyperfine Constants and Spin Density Distribution for a Model $Au_{25}(SH)_{18}$ Nanoparticle Calculated at the LB94/TZP Level of Theory (Since the $[Au_{25}(SR)_{18}]^0$ System has C_i Symmetry, Only the Unique Values are Shown)

Au atom location	A_{iso} (MHz)	spin density
central atom	1.5	0.0564
icosahedral shell	36.0	0.0351
	36.9	0.0374
	37.5	0.0514
	40.0	0.0453
	47.4	0.0371
	56.4	0.0531
six staple motifs	−0.7	0.0023
	2.9	0.0027
	4.8	0.0036
	9.3	0.0112
	12.0	0.0122
	12.5	0.0129

gold atoms near the axis of the superatomic P orbital, whereas the smaller A_{iso} values are for those gold atoms near the node of this orbital. Taken together, the DFT-calculated A_{iso} constants of <100 MHz agree well with the EPR-determined A_{iso} values and thus are compatible with the absence of hyperfine structure in the EPR signal.

The fact that the unpaired spin has a P-state nature and is highly delocalized over the nanoparticle provides an interpretation of the absence of spin−nuclear hyperfine interactions. It is of great interest to map out the unpaired spin in the particle. To study this, we calculated the spin density distribution (Table 1, right column). The results show that gold atoms in the staple motifs do not have significant spin density; instead, the spin density is primarily concentrated in the Au_{13} core. This conclusion is in striking contrast with the results of previous work suggesting that magnetism in gold arises from the particle surface via charge transfer in Au−S bonds (i.e., resulting in 5d localized holes in gold)[3,4,20,21] or from unpaired electrons in the sulfur atom for the Au−thiol SAM system.[22] In the $Au_{25}(SR)_{18}$ system, the three Au atoms in the icosahedral shell that possess the largest spin densities (0.0531, 0.0514, 0.0453) and the one at the center of the icosahedron (spin density 0.0564) form an axis that is consistent with the axial symmetry of the EPR signals. These three atoms (and their inversion-symmetric counterparts) are the primary contributors to the singly occupied HOMO orbital. Other atoms in the Au_{13} core have relatively smaller spin densities (0.035 to 0.037). Overall, the highly delocalized spin density is consistent with the superatom picture wherein the Au_{13} icosahedron possesses a delocalized electronic structure while the outer shell (Au_{12}) forms strong covalent bonding with the thiolates to protect the particle. This is in good agreement with the divide-and-protect concept proposed by Häkkinen et al.[23] These results suggest that the $Au_{25}(SR)_{18}$ nanoparticle can indeed be considered as a superatom. The superatom concept was originally proposed for gas-phase naked metal clusters. Recently, Häkkinen and co-workers[16] extended the superatom picture to account for the closed electronic shell structure of gold−phosphine and gold−thiolate clusters.

Taken together, the results of this work unambiguously demonstrate the intrinsic magnetism in the $Au_{25}(SR)_{18}$ nanoparticles and that the paramagnetism is reversibly switchable through control of the charge state of the nanoparticle. DFT calculations reveal that the unpaired spin is mainly distributed in the Au_{13} core and exhibits axial character. EPR studies imply unusual magnetic properties of the particle in which hyperfine splitting plays little or no role as a result of the P-state nature of the unpaired spin density and its delocalization over many gold atoms. All of these results suggest that the $Au_{25}(SR)_{18}$ nanoparticle is best considered as a ligand-protected superatom. The intrinsic magnetism in the $[Au_{25}(SR)_{18}]^0$ nanoparticles and the reversible switching render these nanoparticles particularly useful as paramagnetic probes. In addition, this study provides a foundation for understanding the size dependence of magnetism in gold nanoparticles that should be amenable to further analysis using crystallographically characterized nanoparticles and electronic structure theory.

Acknowledgment. G.C.S. acknowledges NSF Grant CHE-0550497. C.M.A. acknowledges startup funding from Kansas State University. M.P.H. acknowledges NIH Grant GM 77387. R.J. acknowledges CMU startup funding and Air Force Grant 9550-07-1-0245.

Supporting Information Available: Experimental details. This material is available free of charge via the Internet at http://pubs.acs.org.

References

(1) White, R. M. *Quantum Theory of Magnetism*, 3rd Ed.; Springer: New York, 2007.
(2) Hori, H.; Teranishi, T.; Nakae, Y.; Seino, Y.; Miyake, M.; Yamada, S. *Phys. Lett. A* **1999**, *263*, 406.
(3) Crespo, P.; Litrán, R.; Rojas, T. C.; Multigner, M.; de la Fuente, J. M.; Sánchez-Lopez, J. C.; Garcı´a, M. A.; Hernando, A.; Penadés, S.; Fernández, A. *Phys. Rev. Lett.* **2004**, *93*, 087204.
(4) Hori, H.; Yamamoto, Y.; Iwamoto, T.; Miura, T.; Teranishi, T.; Miyake, M. *Phys. Rev. B* **2004**, *69*, 174411.
(5) Garitaonandia, J. S.; Insausti, M.; Goikolea, E.; Suzuki, M.; Cashion, J. D.; Kawamura, N.; Ohsawa, H.; Gil de Muro, I.; Suzuki, K.; Plazaola, F.; Rojo, T. *Nano Lett.* **2008**, *8*, 661.
(6) Dutta, P.; Pal, S.; Seehra, M. S.; Anand, A.; Roberts, C. B. *Appl. Phys. Lett.* **2007**, *90*, 213102.
(7) Negishi, Y.; Tsunoyama, H.; Suzuki, M.; Kawamura, N.; Matsushita, M. M.; Maruyama, K.; Sugawara, T.; Yokoyama, T.; Tsukuda, T. *J. Am. Chem. Soc.* **2006**, *128*, 12034.
(8) Iwasa, T.; Nobusada, K. *Chem. Phys. Lett.* **2007**, *441*, 268.
(9) Knight, W. D.; Clemenger, K.; de Heer, W. A.; Saunders, W. A.; Chou, M. Y.; Cohen, M. L. *Phys. Rev. Lett.* **1984**, *52*, 2141.
(10) Bergeron, D. E.; Roach, P. J.; Castleman, A. W., Jr.; Jones, N. O.; Khanna, S. N. *Science* **2005**, *307*, 231.
(11) Thomas, O. C.; Zheng, W. J.; Bowen, K. H. *J. Chem. Phys.* **2001**, *114*, 5514.
(12) Luo, W.; Pennycook, S. J.; Pantelides, S. T. *Nano Lett.* **2007**, *7*, 3134.
(13) Zhu, M.; Aikens, C. M.; Hollander, F. J.; Schatz, G. C.; Jin, R. *J. Am. Chem. Soc.* **2008**, *130*, 5883.
(14) Zhu, M.; Eckenhoff, W. T.; Pintauer, T.; Jin, R. *J. Phys. Chem. C* **2008**, *112*, 14221.
(15) Moore, C. E. *Natl. Bur. Stand. Circ. (U.S.)* **1958**, *3*, 467.
(16) Walter, M.; Akola, J.; Lopez-Acevedo, O.; Jadzinsky, P. D.; Calero, G.; Ackerson, C. J.; Whetten, R. L.; Grönbeck, H.; Häkkinen, H. *Proc. Natl. Acad. Sci. U.S.A.* **2008**, *105*, 9157.
(17) Bieron, J.; Fischer, C. F.; Jonsson, P.; Pyykko, P. *J. Phys. B* **2008**, *41*, 115002.
(18) Yulikov, M.; Sterrer, M.; Heyde, M.; Rust, H.-P.; Risse, T.; Freund, H.-J.; Pacchioni, G.; Scagnelli, A. *Phys. Rev. Lett.* **2006**, *96*, 146804.
(19) Kasai, P. H. *J. Am. Chem. Soc.* **1983**, *105*, 6704.
(20) Zhang, P.; Sham, T. K. *Phys. Rev. Lett.* **2003**, *90*, 245501.
(21) Gonzalez, C.; Simon-Manso, Y.; Marquez, M.; Mujica, V. *J. Phys. Chem. B* **2006**, *110*, 687.
(22) Carmeli, I.; Leitus, G.; Naaman, R.; Reich, S.; Vager, Z. *J. Chem. Phys.* **2003**, *118*, 10372.
(23) Hakkinen, H.; Walter, M.; Gronbeck, H. *J. Phys. Chem. B* **2006**, *110*, 9927.

JA809157F